Chinese Journal of Oceanology and Limnology
Vol. 30 No. 6, P. 1105-1115, 2012
http://dx.doi.org/10.1007/s00343-012-1272-y

Effects of spectral nudging on the 2010 East Asia summer monsoon using WRF model*

SHAN Haixia (单海霞)[1, 2], GUAN Yuping (管玉平)[2, **], HUANG Jianping (黄建平)[1]

[1] *Key Laboratory for Semi-Arid Climate Change of the Ministry of Education, College of Atmospheric Science, Lanzhou University, Lanzhou 730000, China*

[2] *State Key Laboratory of Tropical Oceanography, South China Sea Institute of Oceanology, Chinese Academy of Sciences, Guangzhou 510301, China*

Received Dec. 18, 2011; accepted in principle Feb. 6, 2012; accepted for publication Jul. 7, 2012

Abstract The performance of spectral nudging in an investigation of the 2010 East Asia summer monsoon was assessed using the Weather Research and Forecasting (WRF) model, forced by 1-degree NCEP Global Final Analysis (FNL). Two pairs of experiments were made, spectral nudging (SP) and non-spectral nudging (NOSP), with five members in each group. The members were distinguished by different initial times, and the analysis was based on the ensemble mean of the two simulation pairs. The SP was able to constrain error growth in large-scale circulation in upper-level, during simulation, and generate realistic regional scale patterns. The main focus was the model ability to simulate precipitation. The Tropical Rainfall Measuring Mission (TRMM) 3B42 product was used for precipitation verification. Mean precipitation magnitude was generally overestimated by WRF. Nevertheless, SP simulations suppressed overestimation relative to the NOSP experiments. Compared to TRMM, SP also improved model simulation of precipitation in spatial and temporal distributions, with the ability to reproduce movement of rainbands. However, extreme precipitation events were suppressed in the SP simulations.

Keyword: downscaling; regional climate model; East Asia summer monsoon; spectral nudging

1 INTRODUCTION

In recent years, regional climate model (RCM) studies have been greatly developed, and have become one of the most popular endeavors in climate modeling research. In general, spatial resolution of global climate models (GCMs) is relatively low (hundreds of kilometers), and regional features cannot be described very accurately because of their coarse resolutions. Downscaling is an effective means to overcome difficulties of regional climate simulation with GCMs. Dynamical downscaling is a method for obtaining high-resolution climate or climate change information over a region of interest (McGregor, 1997; Giorgi and Mearns, 1999), from either relatively coarse-resolution GCMs or global reanalysis. RCMs have many sources of model errors, such as numerical approximations and limited resolution, parameterization of subgrid-scale physical effects, and limited description of geophysical fields (Laprise et al., 2008), just as with GCMs. RCMs have to deal with the problem of lateral boundary conditions (LBCs), which are a potential external error source (McDonald, 1999). Recent studies have also shown that RCMs exhibit internal variability (IV) (Giorgi and Bi, 2000; Caya and Biner, 2004; Alexandru et al., 2009). RCMs are very sensitive to circulation errors in fields that drive them (Laprise et al., 2008). When errors in an area persist or accumulate to a certain point, they contaminate other model aspects and degrade results elsewhere in the regional domain (Miguez-Macho et al., 2005).

It has been a challenge to balance the performance of RCMs, when simultaneously adding small-scale features and retaining large-scale features. There are

* Supported by the Knowledge Innovation Program of Chinese Academy of Sciences (No. KZCX2-YW-Q11-02)

** Corresponding author: guan@scsio.ac.cn

two common methods to address this problem. One is to subdivide long-term continuous integration into a sequence of short-term simulations in weather forecasting mode (Dickinson et al., 1989; Ji and Vernekar, 1997; Pan et al., 1999; Druyan et al., 2001; Qian et al., 2003; Lo et al., 2008). A problem of this method is that it takes a few hours to a few days for the driving initial and lateral boundary conditions to reach dynamical equilibrium. An alternative approach is spectral nudging (von Storch et al., 2000; Miguez-Macho et al., 2004, 2005; Castro et al., 2005; Radu et al., 2008; Alexandru et al., 2009; Zahn et al., 2008; Kang et al., 2005; Cha et al., 2008, 2009, 2011). It is achieved by adding a new term to tendencies of the variables, which relaxes a selected part of the spectrum to corresponding waves from reanalysis or GCMs. Nudging is confined to upper atmospheric levels above the boundary layer, for prognostic fields like geopotential height, winds, and temperature. In this way, variability of synoptic scale circulation features can be maintained during integration, while allowing RCMs to add value at smaller scales. In this work, we use the spectral nudging technique of Miguez-Macho et al. (2005), recently implemented in the Weather Research and Forecasting (WRF) model.

The East Asian summer monsoon (EASM) is a distinctive component of the Asian climate system, which affects flood and drought over large parts of the Philippines, China, Korea, and Japan. Seasonal variation of heavy precipitation associated with large-scale circulation is one of the dominant characteristics of the EASM. It is still a challenging task to simulate monsoon precipitation accurately, although our understanding of the EASM has improved significantly over the past few decades. Miguez-Macho et al. (2004) showed that spectral nudging of long waves could eliminate non-physical dependence of regional modeling results (especially precipitation) on the position and the size of domain. There have been many studies on the impact of spectral nudging on modeling of EASM precipitation. Models used in these studies include the fifth-generation Pennsylvania State University-National Center for Atmospheric Research Mesoscale Model (PSU-NCAR MM5) (Tang et al., 2010; Gao et al., 2011; Song et al., 2011), Seoul National University Regional Climate Model (SNURCM) (Lee et al., 2004; Kang et al., 2005; Cha et al., 2008, 2009), NCEP regional spectral model (RSM) (Kang and Hong, 2008) and WRF (Cha et al., 2011). It was shown that spectral nudging can help improve model performance not only in simulating mean features, but also in capturing extreme summer precipitation events over East Asia. However, use of spectral nudging remains an open issue. Alexandru et al. (2009) raised concern that application of such nudging could suppress proper generation of fine-scale features. Many previous studies focused on investigating downscaling of East Asian climatology and the special case of a 1998 severe flood in the Changjiang River basin. Here, we focus on another case in 2010, which saw the second most severe flood since 1955 in that basin. This case has yet to be studied.

We focus on discussing preliminary results of dynamically downscaling National Centers for Environmental Prediction (NCEP) Global Final Analysis (FNL) data from the summer of 2010. Section 2 displays basic features of atmospheric circulation in 2010 from NCEP reanalysis. The numerical model and experimental design are described in Section 3. In Section 4, model results are compared to data from the NCEP FNL and Tropical Rainfall Measuring Mission (TRMM), to examine the performance of spectral nudging on simulation of large scale circulation and precipitation. Section 5 provides discussion, and conclusions follow in Section 6.

2 OBSERVED FEATURES OF EASM IN 2010

There were many extreme events in 2010, which resulted from uneven spatial and temporal distributions of precipitation. In Southwest China there was severe drought, while in the middle and lower reaches of the Changjiang River there was flooding, so we choose the latter to investigate whether spectral nudging can improve simulation of EASM circulation and precipitation. Basic features of atmospheric circulation were obtained from NCEP/NCAR reanalysis data (Kalnay et al., 1996).

To arrive at anomalies, a 30-year average from 1971 to 2000 was used as climatology. Fig.1 shows a latitude-height distribution of zonal wind for climatology of May-June-July-August (MJJA) (a), and anomaly (b) in 2010. The axis of the climatological westerly jet at 200 hPa is near 40°N, with maximum speed greater than 20 m/s. In 2010 the axis had a slight southward displacement. There was a negative anomaly at mid latitudes, and positive ones in the subtropics and high latitudes. Results of air temperature are illustrated in Fig.2. The temperature decreased upward (and poleward) until 100 hPa, and

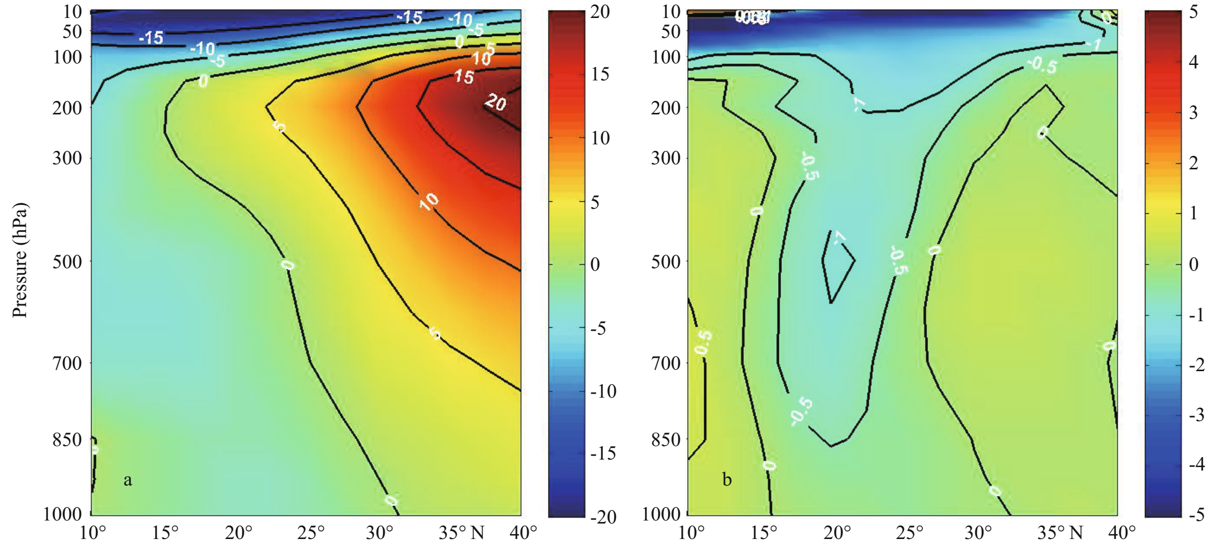

Fig.1 Latitude-height cross section of (a) zonal wind for climatology, and (b) anomaly in 2010 (units: m/s)

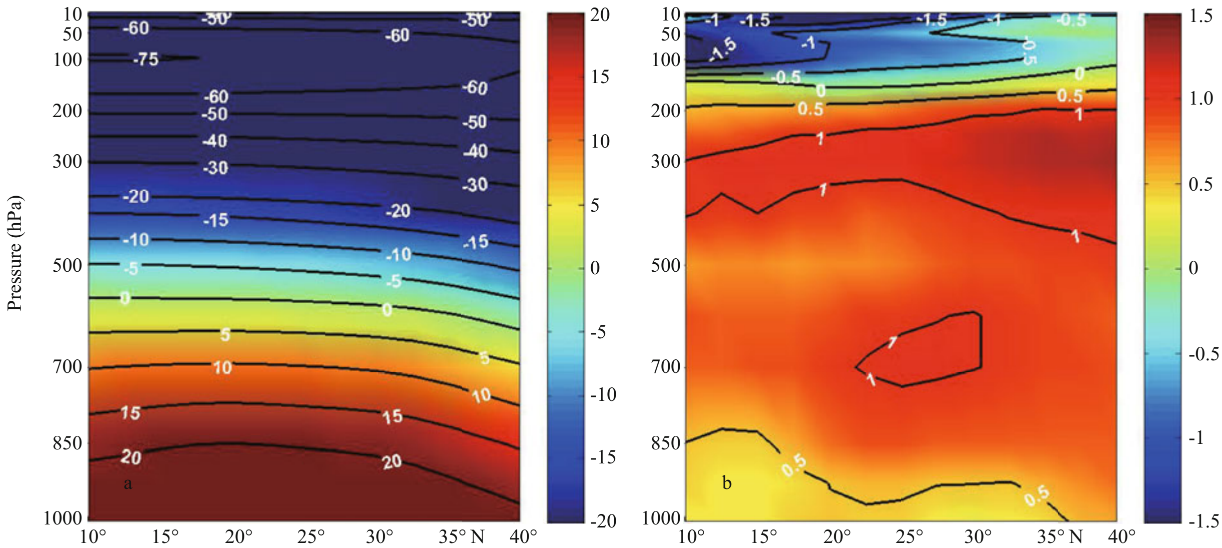

Fig.2 Same as Fig.1, but for air temperature (units: °C)

had an opposite tendency above 100 hPa. It had a colder pattern in layers above 100 hPa, and was warmer than normal years during 2010 in the troposphere. In the surface layer, the air temperature increase at mid latitudes was greater than that in the tropics and subtropics, which made the meridional temperature gradient decrease. The position and intensity of the West Pacific Subtropical High (WPSH) greatly influenced EASM climate. Figure 3 displays 500-hPa geopotential height, for the MJJA climatology and that in 2010. The WPSH was relatively strong, and extended westward to about 110°E in that year.

3 MODEL DESCRIPTION AND EXPERIMENTAL DESIGN

The WRF model with Advanced Research WRF (ARW) dynamic core version 3.2 (Skamarock et al., 2008) was used. WRF is a next-generation, fully compressible, non-hydrostatic, prognostic model suitable for idealized and realistic numerical simulations of the atmosphere. The model uses a terrain-following, hydrostatic-pressure coordinate in the vertical, and the configuration used here had 27 vertical levels. Levels were unevenly distributed in the vertical, from the surface to 50 hPa (top of the

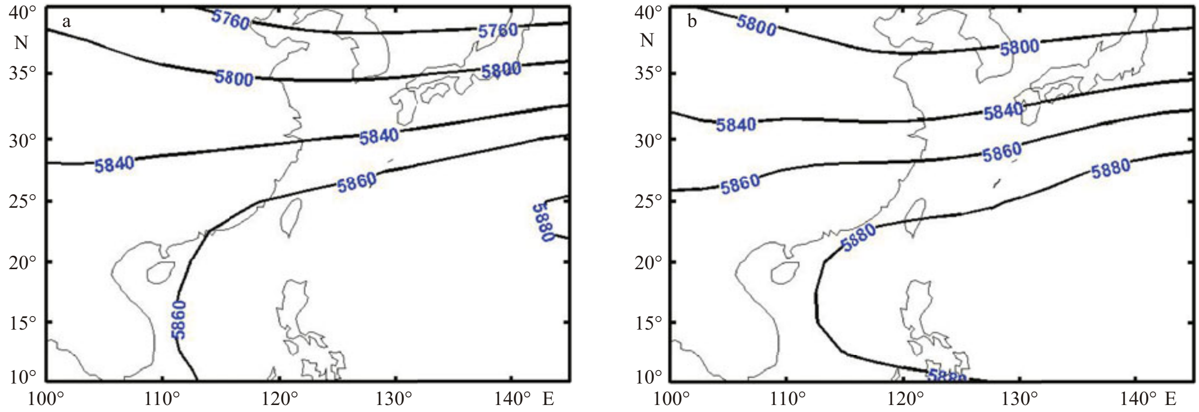

Fig.3 500-hPa geopotential height, for climatology MJJA (a), and that in 2010 (b) (units: m)

model). Over land, the model has four soil layers, and the unified Noah land-surface model was used. The other physical options used include: Rapid Radiative Transfer Model (RRTM) longwave radiation (Mlawer et al., 1997) and Dudhia shortwave radiation (Dudhia, 1989); Lin microphysical parameterization (Lin et al., 1983; Chen and Sun, 2002); Yonsei University (YSU) planetary boundary layer (PBL) scheme (Noh et al., 2003); Betts-Miller-Janjic convective parameterization (Janjic, 2000).

The model domain (Fig.4) was centered at 30°N and 120°E, with 240×180 horizontal grid points. The Mercator map projection was applied, with resolution 30 km. Both spectral nudging and non-spectral nudging experiments were carried out. Each experiment had five members with different initial conditions, spanning five days centered on 1200 UTC 24 April 2010. We hereafter call these SP and NOSP, respectively. In the SP experiments, we applied nudging only on vertical levels above the boundary layer, to *u* and *v* winds, temperature and geopotential height, but not humidity. The threshold for wavelengths above which the waves were nudged was about 1 500 km. We chose a weaker nudging approach (every 24 h) to maximize freedom of the regional model to deviate from global driving fields. Days prior to May 1 were considered a “spin-up” period, and ensemble means of outputs from May 1 to August 31 were analyzed.

Simulations were driven with initial conditions from the 1°×1° FNL, and lateral boundary conditions were updated every six hours. This product is from the Global Data Assimilation System (GDAS), which continuously collects observational data from the Global Telecommunications System (GTS) and other sources, for numerous analyses. Analyses are

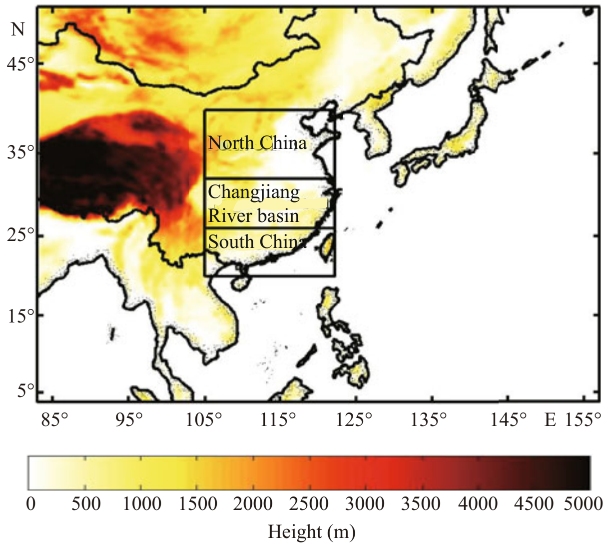

Fig.4 WRF model domain and topography height map

Rectangular boxes denote the regions of South China, Changjiang River basin, and North China.

available on the surface and 26 pressure levels, from 1 000 to 10 hPa. These are available from http://dss.ucar.edu/datasets/ds083.2/. Sea surface temperature (SST) was obtained from daily 0.5-degree NCEP Real Time Global analysis (ftp://polar.ncep.noaa.gov/pub/history/sst) and updated during simulation.

Variables for verification included wind speed at 850 hPa and 200 hPa, geopotential height at 500 hPa, and precipitation. Three-hourly TRMM 3B42 precipitation data (Huffman et al., 2007) were used for precipitation validation, which have spatial resolution 0.25° in the latitude band 50°N–50°S. The dataset used for comparisons of other variables such as wind and geopotential height was the FNL. To facilitate comparison, both TRMM and FNL data were bilinearly interpolated on the WRF grid.

Internal model variability was measured by the spread among ensemble members during simulation, using standard deviation $\sqrt{\sigma_{\mathrm{en}}^2}$ between the five members, which is the same method as Alexandru et al. (2009).

$$\sigma_{\mathrm{en}}^2(i,j,t)=\frac{1}{m}\sum_{m=1}^{M}(X_m(i,j,t)-\langle X\rangle(i,j,t))^2 ,$$

The term X_m (i, j, t) refers to a variable X on grid point (i, j) at time t for member m in the ensemble, and M is the number of ensemble members. The term $X(i, j, t)$ is the ensemble mean, defined as

$$\langle X\rangle(i,j,t)=\frac{1}{m}\sum_{m=1}^{M}X_m(i,j,t) .$$

Differences between individual simulations and observations for a given variable X at given time t were obtained via the spatial root-mean-square difference (RMSD), computed as

$$\mathrm{RMSD}_m(t)=\sqrt{\overline{[X_m(i,j,t)-X_{\mathrm{obs}}(i,j,t)]^2}^{xy}} ,$$

where the xy operator refers to a simple spatial average over the domain. The spatially averaged and time-averaged RMSD of departure of ensemble mean from observations was obtained by computing RMSDs.

To assess the relative magnitude of RMSD of a given variable in the SP and NOSP experiments, the square root of the domain-averaged temporal variance σ of variable X was computed as

$$\sigma=\sqrt{\overline{[\langle X\rangle(i,j,t)-X_{\mathrm{obs}}(i,j,t)]^2}^{xyt}} ,$$

where the xyt operator refers to a 4-month (MJJA) average over the domain. Table 1 gives the exact value.

Table 1 Domain-averaged temporal variance σ for both SP and NOSP simulations

	Wind (200 hpa) (m/s)	Wind (850 hpa) (m/s)	Hgt (500 hpa) (m)	Precipitation (mm/day)
NOSP	3.2	6.8	20.4	14.4
SP	2.0	4.6	15.8	13.5

4 RESULT

4.1 Large-scale variables

The large-scale variables wind speed at 850 hPa and 200 hPa, and geopotential height at 500 hPa were chosen for verification. We selected winds at the foregoing levels because they represent basic features at low and high levels of the atmosphere, and 500 hPa geopotential height reflects large-scale circulation at mid levels. The location and intensity of the WPSH strongly influenced the climate (especially precipitation) during summer monsoon season.

Figures 5 and 6 depict ensemble mean distributions for wind and geopotential height during the four-month simulation (MJJA). There was a large bias of wind speed at 200 hPa simulated by NOSP in northern China and southern part of the domain relative to the NCEP FNL result, whereas for SP this bias was smaller. As for 850 hPa wind speed, bias was mainly in southern China and the South China Sea. The spectral nudging reduced bias, but some positive bias remained. Wind speed at both 850 hPa and 200 hPa was a little stronger than the FNL results. As for 500 hPa geopotential height, there was negative bias over the South China Sea and Tibetan Plateau in the NOSP experiments. In the SP experiments, there was only negative bias over the Tibetan Plateau. Tang et al. (2010) also found that negative bias of 500 hPa geopotential height over this plateau was reduced by SP. Overestimation of geopotential height in the SP experiments was more serious in the southern part of the domain, but when compared with NCEP/NCAR reanalysis data, the bias was not large. Mean geopotential height in NCEP FNL was weaker than that in NCEP/NCAR reanalysis data, which is evident from Fig.3b, 6d. Despite the fact that MJJA mean geopotential height in SP experiments had a greater positive bias relative to that of FNL, domain-averaged temporal variance σ was much smaller relative to NOSP experiments (Table 1).

4.2 Precipitation

Precipitation is an important component of the hydrologic cycle. Correct simulation of monsoon precipitation requires accurate representation of atmospheric circulation, orography, surface properties, radiation processes, parameterization of convection and microphysical cloud processes, plus others. Distributions of daily mean precipitation from TRMM, NOSP and SP experiments are shown in Fig.7. Although the WRF model captured the basic distribution of precipitation, it had a positive bias corresponding to the TRMM data. Mean precipitation magnitude was overestimated in southern China and the Indochina Peninsula in both NOSP and SP simulations, but this bias was reduced with application of spectral nudging. Model overestimation of precipitation in South China was also reported by Tang et al. (2010), in which they had chosen three

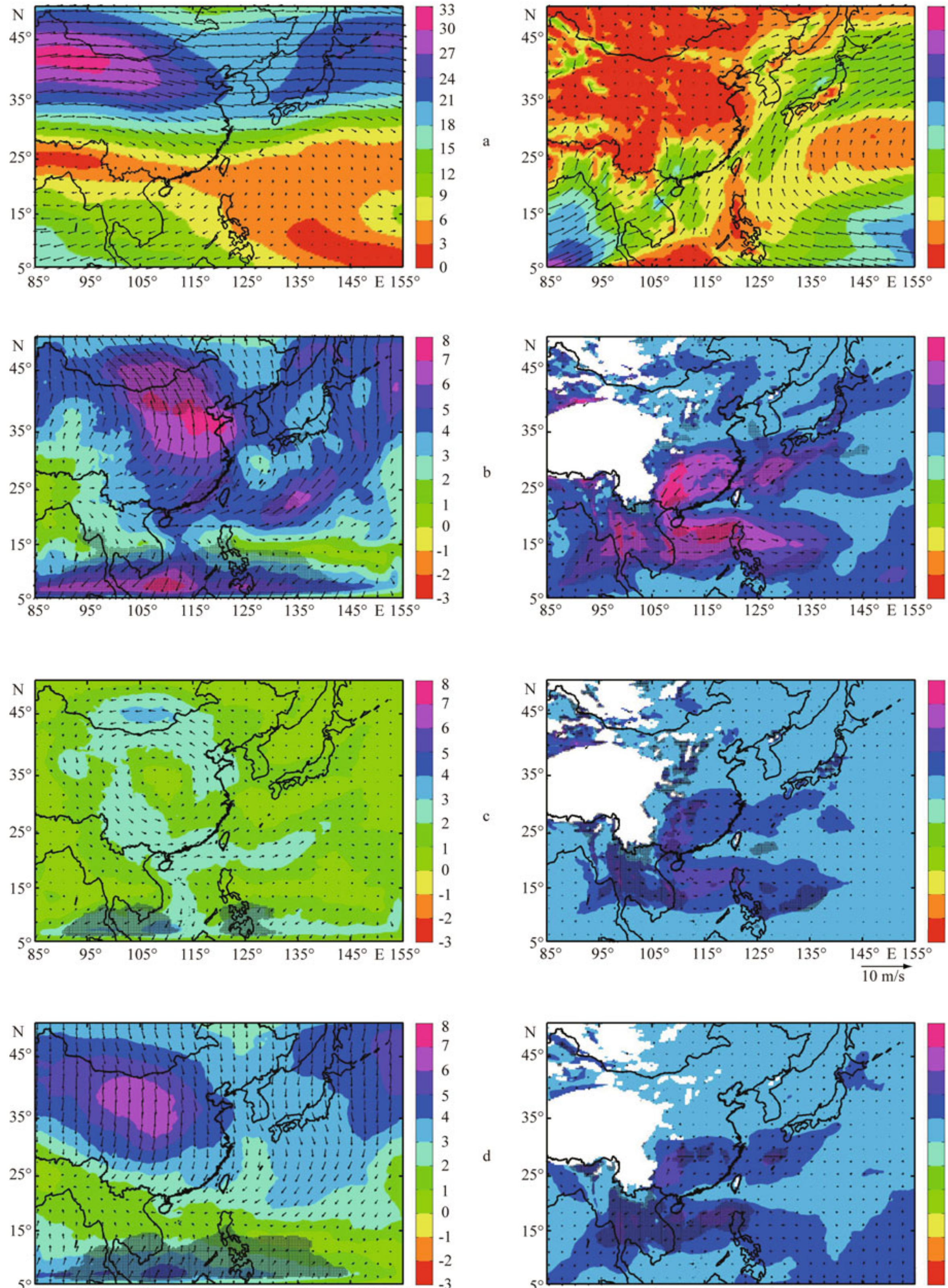

Fig.5 MJJA mean horizontal wind fields (vector; units: m/s) and wind speed (shading; units: m/s) derived from NCEP FNL data (a); differences between NCEP FNL and ensemble mean of NOSP experiments (b); and SP experimental results (c); differences of ensemble mean between SP and NOSP experiments are shown in (d)

Left panel is for wind field at 200 hPa, right one for 850 hPa. Black circles indicate areas with significance at 99% confidence level for wind speed difference, using *t*-test.

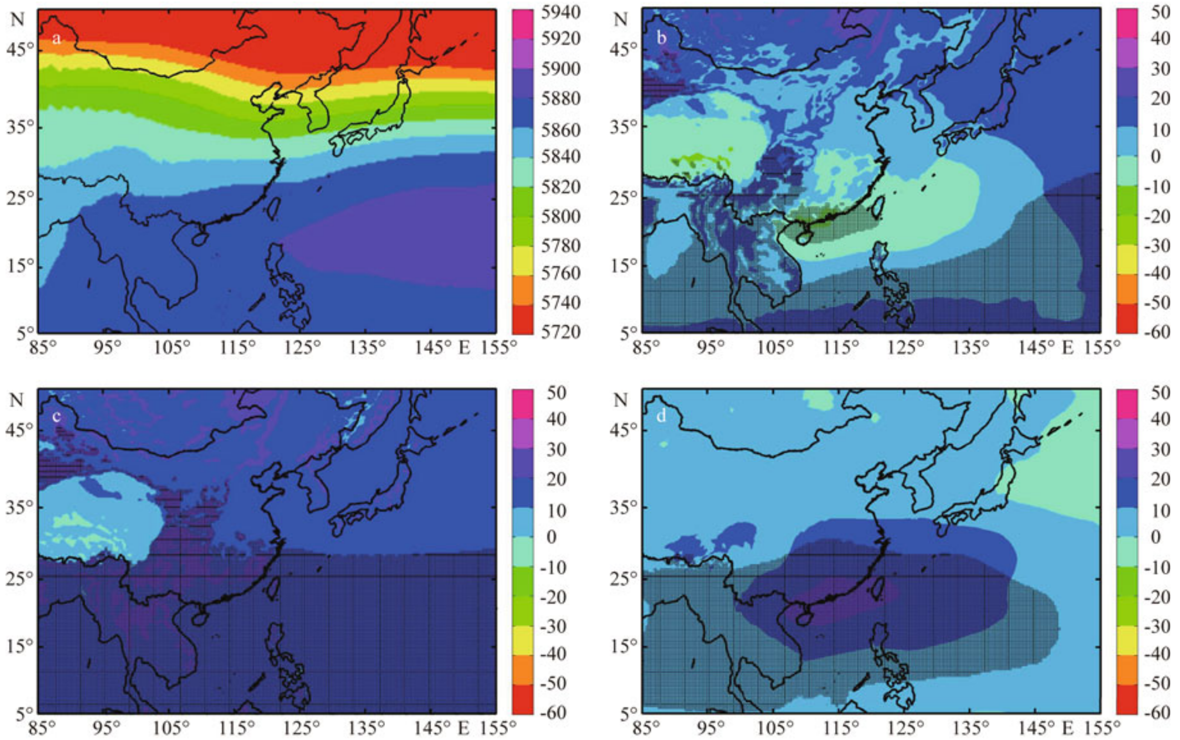

Fig.6 MJJA-mean 500 hPa geopotential height (shading; units: m) derived from NCEP FNL data (a), differences between NCEP FNL and ensemble mean of NOSP experiment (b), and SP experiment result (c). Differences of ensemble mean between SP and NOSP experiments shown in (d)

Black circles indicate areas with significance at 99% confidence level for difference of 500 hPa geopotential height, using *t*-test.

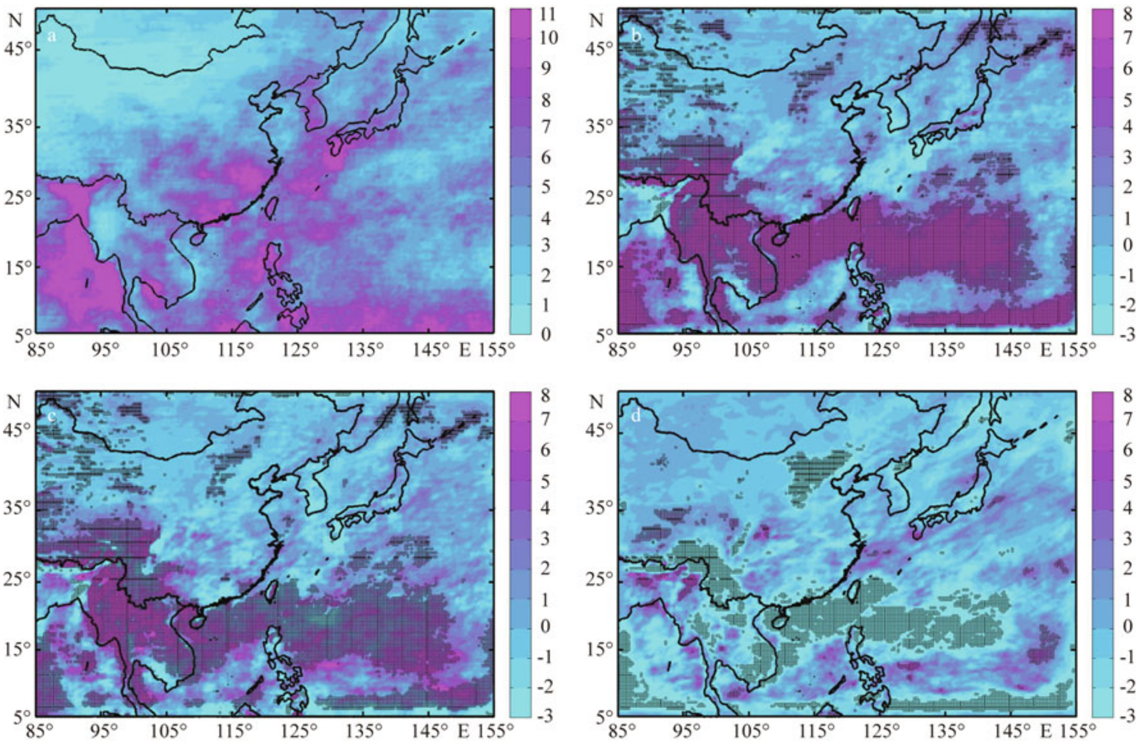

Fig.7 MJJA daily mean precipitation (units: mm/day) derived from TRMM data (a), differences between TRMM and ensemble mean of NOSP experiment (b), and SP experiment result (c). Differences of ensemble mean between SP and NOSP experiments shown in (d)

Black circles indicate areas significant at 99% confidence level for difference of precipitation, using *t*-test.

cases (1991, 1998, and 2003) to study the effect of SP. Figure 8 gives RMSD time series for daily mean precipitation in individual cases of NOSP and SP experiments. We see that RMSD varied because of different initial conditions. In the SP experiments, RMSDs were very close to each other, showing reduced internal model variability in these experiments, which is clearly evident in Fig.8c. Overall, RMSD in the SP experiments was smaller than in the NOSP experiments.

Seasonal translation of the rain belt during monsoon season is one of the main climatic characteristics in eastern China, which determines the basic regional distribution of precipitation. Droughts and floods in this part of the country are related to timing of rain belt shifts and duration over a particular location. To further validate WRF simulation ability for precipitation, we calculated zonally averaged precipitation (105°E–122°E). Figure 9 shows a time-latitude distribution of daily precipitation, from WRF outputs and TRMM observation.

Onset of the East Asian summer monsoon was marked by a period of pre-monsoonal rain over South China and Taiwan Island in late May 2010. In June, rain mainly occurred in South China. The rain band shifted to about 30°N in July, causing heavy rainfall in the southern Changjiang River basin and little rainfall in South China. In late July to August, as WPSH continued to move north, the rain belt was in North China and the South China Sea. In late August, rainbands began to withdraw southward. The northward movement of the rain belt was not simulated well in the NOSP experiments, and precipitation over the South China Sea was too heavy relative to TRMM data. The rain belt lingering in the Changjiang River basin in mid July in the NOSP experiments was not captured. Moreover, mean precipitation in North China during August was much smaller relative to that of TRMM in the SP experiment. Pattern correlation coefficients between observation and each ensemble simulation were also calculated. These were only 0.29 for the NOSP experiments, and 0.56 for the SP experiments. Wang and Yang (2008) also calculated these coefficients using WRF to simulate precipitation in 1998. In their study, the coefficient was 0.50 for the ensemble mean of simulation driven by the mean of NCEP/DOE R2 and ERA40 reanalysis data. After using SP, the coefficient also exceeded 0.5. Caya and Biner (2004) showed that most differences between a pair of simulations result from lack of correlation in temporal evolution

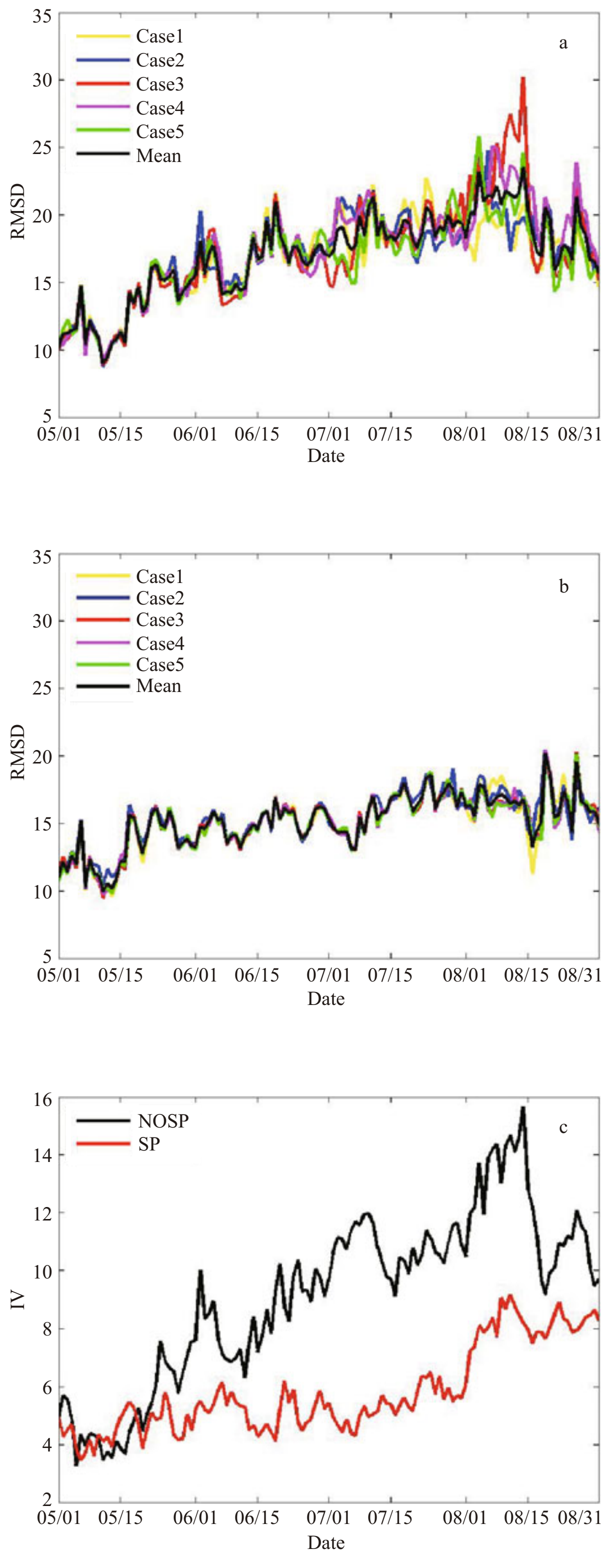

Fig.8 RMSD time series for daily mean precipitation (units: mm/day) in NOSP experiment (a), and SP experiment (b), relative to TRMM. Time evolution of domain-averaged internal variability (IV) is shown in (c)

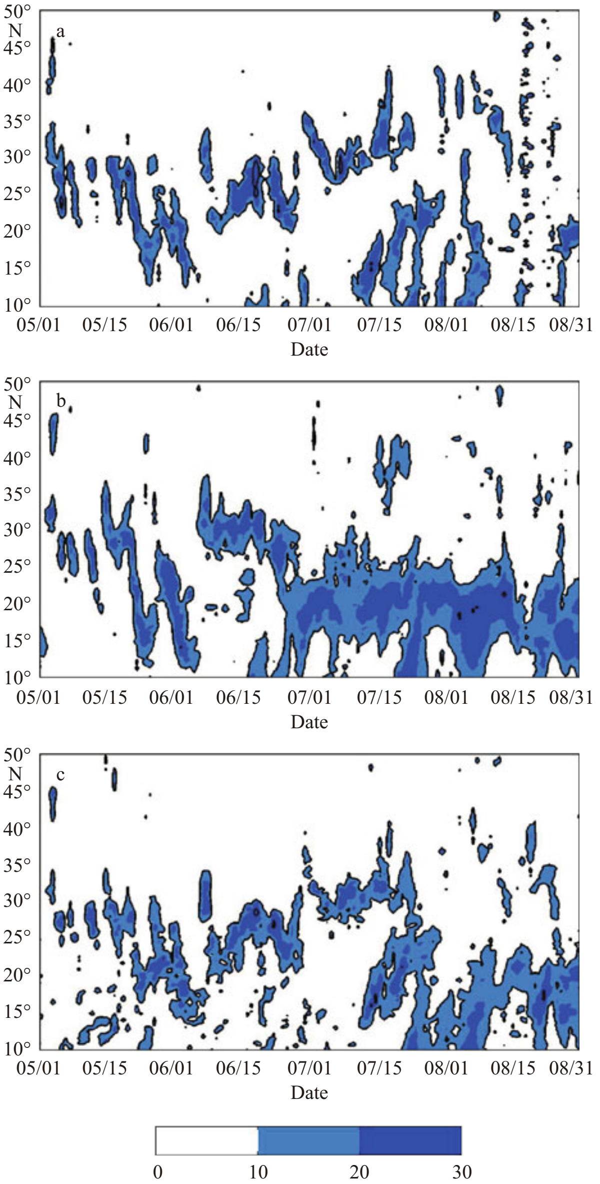

Fig.9 TRMM (a), NOSP experiment (b), and SP experiment (c) outputs in time-latitude distributions of daily precipitation, averaged between 105°E and 122°E (units: mm)

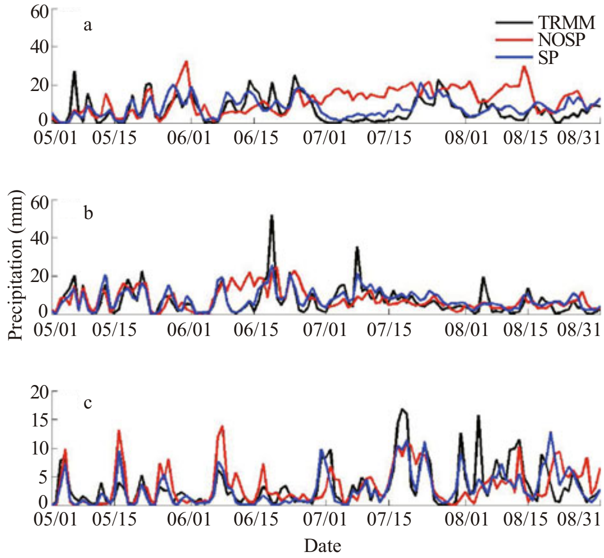

Fig.10 Time series of observed and simulated regional daily ensemble mean precipitation over South China (a), Changjiang River basin (b), and North China (c) during MJJA of 2010 (units: mm)

Table 2 Temporal correlation coefficients of three regional, ensemble-averaged daily precipitation time series relative to TRMM, in SP and NOSP experiments

	North China	Changjiang River basin	South China
NOSP	0.48	0.42	0.12
SP	0.75	0.82	0.73

of the variable.

Figure 10 displays time series of regionally averaged daily precipitation rates in North China (32°–40°N, 105°–122°E), Changjiang River basin (26°–32°N, 105°–122°E) and South China (20°–26°N, 105°–122°E) derived from TRMM, NOSP and SP experiments. Temporal correlation coefficients between TRMM and the two experiments are shown in Table 2. It is obvious that the NOSP simulation produced relatively larger discrepancies, while overestimation was suppressed in the SP experiments. Of the three regions, the simulated result of the NOSP experiments in North China was best (correlation coefficient R=0.48), with that of the Changjiang River basin in second place (R=0.42). Correlation was poorest between observations and NOSP experiments in South China (R=0.12). Correlations between TRMM and the SP experiments were generally better than those between TRMM and NOSP experiments in the three regions. Mean precipitation in the Changjiang River basin was greater than 30 mm on 19 June and 8 July, but the SP experiments did not reproduce these features in that precipitation was underestimated.

5 DISCUSSION

In conventional long-term simulation with only a single initialization of large-scale fields and frequent updating of lateral boundary conditions, the single control of boundaries is insufficient to prevent a certain amount of decorrelation of RCM-simulated fields and driving fields at large scales. The spectral nudging method can mitigate such errors. It imposes a known large-scale state on simulation of regional climate with an RCM, by adding a nudging term to tendencies of the variables that relaxes a selected part of the spectrum to corresponding waves from reanalysis (von Storch et al., 2000). Miguez-Macho et al. (2005) showed that significant errors in a monthly precipitation pattern (June, 2000) within a domain over North America was largely due to systematic distortion of large-scale flow interacting with the lateral boundaries. They found that spectral nudging could eliminate bias in the circulation and greatly improve the precipitation pattern. The WPSH is one of the main atmospheric systems modulating summer precipitation over China. Therefore, simulated precipitation is directly dependent on the model capability to capture WPSH activity and corresponding regional circulations (Zhong, 2006). Spectral nudging produces reasonable WPSH behavior during the summer monsoon season, and improves simulated precipitation. This nudging is a powerful tool for correcting RCM weaknesses such as internal variability, as seen in Fig.8. Moreover, it can reduce sensitivity of regional precipitation patterns to the choice of model domain and grid geometry, while adding small-scale structures (Castro et al., 2005). Consequently, the pattern of precipitation variability in the SP simulation was more consistent with TRMM.

6 CONCLUSION

In this paper, we used the WRF model to downscale coarse-resolution NCEP FNL data onto 30 km grids during the 2010 East Asia summer monsoon. Both spectral nudging and non-spectral nudging experiments were conducted, and each experiment had five members with different initial conditions. By comparing ensemble means of both experiments, we found that application of spectral nudging in WRF simulation improves model downscaling skill. This was true not only for simulating realistic large-scale circulation and mean precipitation, but also for reproducing seasonal variability of precipitation in East Asia. Therefore, this high-resolution model, with realistic surface topography and use of nudging, was able to capture major features of the East Asia Summer Monsoon (EASM). Although SP simulations were constrained by the large-scale circulation, there were still some areas where they performed very poorly for precipitation. The WRF generally overpredicted mean precipitation magnitude. Precipitation results in the SP experiments improved substantially relative to the NOSP simulations, and seasonal movement of major rainbands were also reproduced. However, extreme precipitation events were underestimated in the SP simulations.

References

Alexandru A, de Elia R, Laprise R, Separovic L, Biner S. 2009. Sensitivity study of regional climate model simulations to large-scale nudging parameters. *Mon. Wea. Rev.*, **137**: 1 666-1 686, http://dx.doi.org/10.1175/2008MWR2620.1.

Castro C L, Pielke R A, Leoncini G. 2005. Dynamical downscaling: assessment of value retained and added using the Regional Atmospheric Modeling System (RAMS). *J. Geophys. Res.*, **110**: D05108, http://dx.doi.org/10.1029/2004JD004721.

Caya D, Biner S. 2004. Internal variability of RCM simulations over an annual cycle. *Clim. Dyn.*, **22**: 33-46.

Cha D H, Lee D K, Hong S Y. 2008. Impact of boundary layer processes on seasonal simulation of the East Asian summer monsoon using a regional climate model. *Meteorol. Atmos. Phys.*, **100**: 53-72.

Cha D H, Lee D K. 2009. Reduction of systematic errors in regional climate simulations of the summer monsoon over East Asia and the western North Pacific by applying the spectral nudging technique. *J. Geophys. Res.*, **114**: D14108, http://dx.doi.org/10.1029/2008JD011176.

Cha D H, Jin C S, Lee D K, Kuo Y H. 2011. Impact of intermittent spectral nudging on regional climate simulation using Weather Research and Forecasting Model. *J. Geophys. Res.*, **116**: D10103, http://dx.doi.org/10.1029/2010JD015069.

Chen S H, Sun W Y. 2002. A one-dimensional time dependent cloud model. *J. Meteor. Soc. Jpn.*, **80**: 99-118.

Dickinson R E, Errico R M, Giorgi F, Bates G T. 1989. A regional climate model for the western United States. *Climatic Change*, **15**: 383-422.

Druyan L M, Fulakeza M B, Lonegan P, Saloum M. 2001. A regional model study of synoptic features over West Africa. *Mon. Wea. Rev.*, **129**: 1 564-1 577.

Dudhia J. 1989. Numerical study of convection observed during the winter monsoon experiment using a mesoscale two dimensional model. *J. Atmos. Sci.*, **46**: 3 077-3 107.

GaoY H, Xue Y K, Peng W, Kang H S, Waliser D. 2011. Assessment of dynamic downscaling of the extreme rainfall over East Asia using a regional climate model. *Adv. Atmos. Sci.*, **28**(5): 1 077-1 098, http://dx.doi.org/10.1007/s00376-010-0039-7.

Giorgi F, Mearns L O. 1999. Introduction to special section: regional climate modeling revisited. *J. Geophys. Res.*, **104**(D6): 6 335-6 352.

Giorgi P, Bi X. 2000. A study of internal variability of a regional climate model. *J. Geophys. Res.*, **105**: 29 503-29 521.

Huffman G J, Adler R F, Bolvin D T, Gu G, Nelkin E J, Bowman K P, Hong Y, Stocker E F, Wolff D B. 2007. The TRMM Multi-satellite Precipitation Analysis (TMPA): quasi-global, multi-year, combined-sensor precipitation estimates at fine scale. *J. Hydrometeor*, **8**: 38-55.

Ji Y, Vernekar A D. 1997. Simulation of the Asian summer monsoons of 1987 and 1988 with a regional model nested in a global GCM. *J. Clim*., **10**: 1 965-1 979.

Janjic Z I. 2000. Comments on “Development and evaluation of aconvection scheme for use in climate models”. *J. Atmos*. *Sci*., **57**: 3 686.

Kalnay E, Kanamitsu M, Kistler R, Collins W, Deaven D, Gandin L, Iredell M, Saha S, White G, Woollen J, Zhu Y, Chelliah M, Ebisuzaki W, Higgins W, Janowiak J, Mo K C, Ropelewski C, Wang J, Leetmaa A, Reynolds R, Jenne R, Joseph D. 1996. The NCEP/NCAR 40-year reanalysis project. *Bull*. *Am*. *Meteorol*. *Soc*., **77**(3): 437-471, http://dx.doi.org/10.1175/1520-04 77(1996)077<0437:TNYRP>2.0.CO;2.

Kang H S, Cha D H, Lee D K. 2005. Evaluation of the mesoscale model/land surface model (MM5/LSM) coupled model for East Asian summer monsoon simulations. *J. Geophys*. *Res*., **110**: D10105, http://dx.doi.org/10.1029/2004JD005266.

Kang H S, Hong S Y. 2008. An assessment of the land surface parameters on the simulated re-gional climate circulations: the 1997 and 1998 east Asian summer monsoon cases. *J. Geophys*. *Res*., **113**: D15121, http://dx.doi.org/10.1029/2007JD009499.

Laprise R, de Elia R, Caya D, Biner S, Lucas-Picher P, Diaconescu E, Leduc M, Alexandru A, Separovic L, Canadian Network for Regional Climate Modelling and Diagnostics. 2008. Challenging some tenets of Regional Climate Modelling. *Meteor*. *Atmos*. *Phys*., **100**: 3-22.

Lin Y L, Farley R D, Orville H D. 1983. Bulk parameterization of the snow field in a cloud model. *J. Clim*. *Appl*. *Meteor*., **22**: 1 065-1 092.

Lee D K, Cha D H, Kang H S. 2004. Regional climate simulation of the 1998 summer flood over East Asia. *J. Meteorol*. *Soc*. *Jpn*., **82**(6): 1 735-1 753.

Lo J C F, Yang Z L, Pielke R A. 2008. Assessment of three dynamical climate downscaling methods using the Weather Research and Forecasting (WRF) model. *J. Geophys*. *Res*., **113**: D09112, http://dx.doi.org/10.1029/2007JD009216.

McGregor J L. 1997. Regional climate modelling. *Meteor*. *Atmos*. *Phys*., **63**: 105-117.

McDonald A. 1999. A review of lateral boundary conditions for limited area forecast models. *Proc*. *Ind*. *Natl*. *Sci*. *Acad*., **65**: 91-105.

Miguez-Macho G, Stenchikov G L, Robock A. 2004. Spectral nudging to eliminate the effects of domain position and geometry in regional climate model simulations. *J. Geophys*. *Res*., **109**: D13104, http://dx.doi.org/10.1029/2003JD004495.

Miguez-Macho G, Stenchikov G L, Robock A. 2005. Regional climate simulations over North America: interaction of local processes with improved large-scale flow. *J. Clim*., **18**: 1 227-1 246.

Mlawer E J, Taubman S J, Brown P D, Iacono M J, Clough S A. 1997. Radiative transfer for inhomogeneous atmospheres: RRTM, a validated correlated-k model for the long wave. *J. Geophys*. *Res*., **102**(D14): 16 663-16 682.

Noh Y, Cheon W G, Hong S Y, Raasch S. 2003. Improvement of the K-profile model for the planetary boundary layer based on large eddy simulation data. *Boundary-Layer*. *Meteorol*., **107**: 401-427.

Pan Z, Takle E, Gutowski W, Turner R. 1999. Long simulation of regional climate as a sequence of short segments. *Mon*. *Wea*. *Rev*., **127**: 308-321.

Qian J H, Seth A, Zebiak S. 2003. Reinitialized versus continuous simulations for regional climate downscaling. *Mon*. *Wea*. *Rev*., **131**: 2 857-2 874.

Skamarock W C, Klemp J B, Dudhia J, Gill D O, Barker M, Duda K G, HuangX Y, Wang W, Powers J G. 2008. A description of the Advanced Research WRF Version 3. NCAR/TN-475+STR, NCAR TECHNICAL NOTE. 113p.

Song S, Tang J P, Chen X. 2011. Impacts of spectral nudging on the sensitivity of a regional climate model to convective parameterizations in East Asia. *Acta Meteor*. *Sinica*, **25**(1): 63-77, http://dx.doi.org/10.1007/s13351-011-0005-z.

Tang J P, Song S, Wu J A .2010. Impacts of the spectral nudging technique on simulation of the East Asian summer monsoon. *Theor*. *Appl*. *Climatol*., **101**(12): 41-51, http://dx.doi.org/10.1007/s00704-009-0202-1.

Radu R, Deque M, Somot S, 2008. Spectral nudging in a spectral regional climate model. *Tellus*, **60A**: 898-910.

von Storch H, Langenberg H, Feser F. 2000. A spectral nudging technique for dynamical downscaling purposes. *Mon*. *Wea*. *Rev*., **128**: 3 664-3 673.

Wang B, Yang H. 2008. Hydrological issues in lateral boundary conditions for regional climate modeling: simulation of East Asian summer monsoon in 1998. *Clim*. *Dyn*., **31**: 477-490.

Zahn M, Von Storch H, Bakan S. 2008. Climate mode simulation of North Atlantic polar lows in a limited area model. *Tellus*, **60A**: 620-631.

Zhong Z. 2006. A possible cause of a regional climate model's failure in simulating the east Asian summer monsoon. *Geophys*. *Res*. *Lett*., **33**: L24707, http://dx.doi.org/10.1029/2006GL027654.